One-dimensional model of the plasma flow in a Hall thruster

E. Ahedo and P. Martínez-Cerezo
E.T.S.I. Aeronáuticos, Univ. Politécnica, 28040 Madrid, Spain

M. Martínez-Sánchez
Massachusetts Institute of Technology, Cambridge, Massachusetts 02139

(Received 19 January 2001; accepted 20 March 2001)

A macroscopic model which accounts for the complex interactions between electrostatic, thermal, and kinetic effects in a Hall thruster is presented. The analysis establishes the one-dimensional steady structure of the flow as consisting of an anode sheath, a long electron free-diffusion region, with reverse ion flow, a thin ionization layer, and the acceleration region, which extends into the plume. The ion flow presents a forward sonic point around the exit of the ionization layer, which can be either internal, with a smooth sonic transition, or localized at the channel exit. The supersonic plume is included via a simple expansion model, allowing closure of the formulation and calculation of thruster performance. The results indicate good agreement with experimental data for the case of an internal sonic point, and they delineate the existence and nonexistence regions in the space of externally controllable parameters. They also unveil the importance of the electron pressure, the reverse flow of ions, and the ionization rate in shaping the plasma structure, whereas, contrary to common perception, the details of the magnetic field profile influence weakly that structure. © *2001 American Institute of Physics.* [DOI: 10.1063/1.1371519]

I. INTRODUCTION

The very simplicity of the Hall thruster structure, with no screens or other control surfaces, makes it difficult to understand the interrelationships which, in the end, localize and shape the various plasma regions existing in the accelerating channel. Bishaev and Kim[1] distinguish, in their experiments, (i) an upstream diffusion region, with negligible electric field, no ion production, predominant ion motion towards the anode, and low plasma temperature ($\sim 3-6$ eV); (ii) an intense ionization layer, placed near the channel exit, with peaks of plasma density and temperature ($\sim 20-30$ eV); and (iii) an acceleration region, where most of the potential drop takes place, and extending outside the channel into the plume. These characteristics of the plasma flow are confirmed by other experimental observations[2,3] and by two-dimensional (2-D) plasma simulations.[4] Since the radial magnetic field is usually shaped with a peak near the channel exit, the above plasma structure has often been explained as simply a reflection of the magnetic field distribution.

A recent review paper on Hall thruster physics[5] recognizes that there is still no model describing adequately the plasma dynamics inside the accelerating channel. The importance of developing a reliable model that improves our understanding of the factors which control plasma structure becomes evident when we attempt to improve upon existing Hall thruster designs, particularly regarding (i) thrust efficiency, (ii) erosion, and (iii) control of oscillations. Present design criteria are based mainly on testing experience. Erosion of the thruster walls is the main factor limiting the thruster lifetime. The erosion rate is governed by local plasma density, electron temperature, and sheath drop, and each of these may show order-of-magnitude variations within the channel making it crucial to have theoretical guidance for steering their peaks to the least damaging locations possible. Plasma self-oscillations are manifested by a modulation of the discharge current in the range 10–100 kHz for thrusters in the 1 kW range.[6,7] This modulation can be fairly deep, up to a full 100%, but at other times it is much weaker or almost absent, and the reasons for these widely different behaviors are not understood at present.

In this paper we present a 1-D macroscopic model of the plasma response inside the thruster and in the near plume. In an intended balance of simplicity and reliability the model presents, of necessity, simplifications in several respects (most notably in their 1-D structure), but it contains still enough basic physics to illuminate the complex interplay of phenomena which shape the Hall thruster plasma. Of course, we do not pretend quantitative accuracy in the predictions of such a model. Emphasis will be given to the consistency of the governing equations and their boundary conditions, to the understanding of the physical processes that govern each plasma region, and to the identification of the different types of solutions that can appear. The model will show that the fluid-like response of the plasma can, by itself and nearly independent of the magnetic structure, explain many of the features observed in experiments.

Several models of the channel have been proposed previously; Refs. 8–11 are some of them. In general, emphasis has been on achieving a satisfactory performance prediction, which, if a few reasonable assumptions are introduced about the flow structure, is not too difficult to achieve (particularly regarding thrust). However, published models fail to describe the whole plasma structure and dynamics. For instance, none of them recovers correctly the diffusion region (which occupies most of the channel) and the crucial role there of the

 © 2001 American Institute of Physics

Downloaded 07 Jun 2001 to 138.4.73.144. Redistribution subject to AIP license or copyright, see http://ojps.aip.org/pop/popcr.jsp

electron pressure (confirmed by experimental data[1]). Plume models form a separate group and are generally focused in the far-field region, downstream of the beam neutralization.[12,13] Partial versions of the model analyzed here were presented in recent Conferences on Electric Propulsion.[14–16]

The paper is organized as follows. In Sec. II we present a complete discussion of the model, including basic simplifications, modelization of the different phenomena, characteristics of the mathematical model, and boundary conditions. In Sec. III we discuss the different types of solutions obtained from the integration of the equations, showing which is the most plausible kind. In Sec. IV we comment on the main features of the plasma response along the different spatial regions. In Sec. V we derive an asymptotic solution of the plasma response which explains the physics that governs the plasma response. In Sec. VI we discuss the main results and points out desirable improvements.

II. FORMULATION OF THE MODEL

Geometrical sketches of the thruster and the main features of the 1-D model are drawn in Figs. 1(a) and 1(b). The 1-D hypothesis implies that all physical magnitudes in channel and plume are averaged radially. The channel is of length L and has a constant radial area A_c (and radial thickness h_c); we take $x_A=0$ at the anode, and $x_E=L$ at the channel exit. The plume is modeled as a divergent channel with a radial area $A(x)$, which will be determined as part of the solution. The magnetic field is assumed radial with a Gaussian axial profile,

$$B(x)=B_m \exp\left[-\frac{(x-x_m)^2}{L_m^2}\right], \tag{1}$$

where B_m, x_m, and L_m are constants, with x_m close to x_E [there is no difficulty in using more accurate expressions of $B(x)$ but Eq. (1) is sufficient for the purposes of this paper]. In this 1-D model electrons are injected into the plasma plume through a virtual cathode (point P) placed at a distance $L_{EP}(=x_P-x_E)$ from the channel exit. The voltage difference between points A and P is the discharge voltage $V_d=\phi_A-\phi_P$, and the electron current delivered by the cathode is the discharge current I_d. One part of this current diffuses inwards (into the near plume), across the magnetic field lines, and ionizes the mass flow of neutrals, $\dot{m}$, emitted at the anode. The other part of the electron current flows outwards (into the far plume) and neutralizes the ion current; subscript ∞ will refer to downstream conditions far away from the cathode. To facilitate this flow of electrons out of the cathode the voltage profile, $\phi(x)$, is expected to be minimum at point P. The voltage difference $\phi_\infty-\phi_P>0$ can be interpreted as the cost of the electron emission.

Since the Debye length is generally very small (of the order of $10-100\,\mu$m) compared to the channel length, the plasma is considered quasineutral everywhere except in an electron-repelling sheath attached to the anode; this is region AB in Fig. 1, with point B marking the transition to the sheath. In this sheath, a self-adjusted potential bias, $\phi_{\rm sh}=\phi_B-\phi_A>0$, equates the electron thermal flow collected at

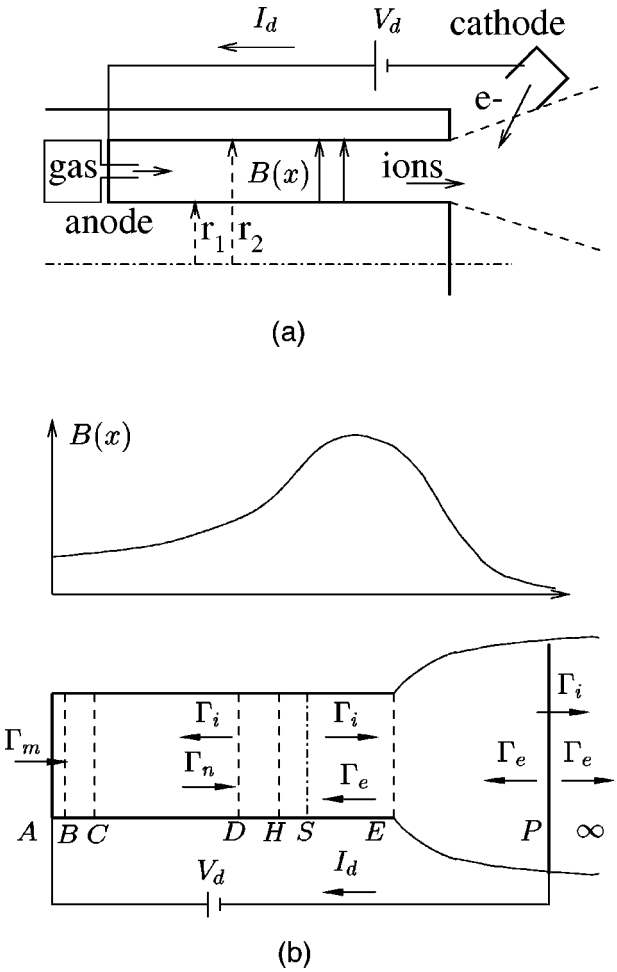

FIG. 1. Sketches of (a) the Hall thruster and (b) the 1-D macroscopic model. $B(x)$ is the magnetic field profile; V_d is the discharge voltage; I_d the discharge current; $\dot{m}$ the flow of neutral gas; Γ_α, $\alpha=i,e,\ldots$, are particle flows of the different species. Surface P is the cathode (beam neutralizer). For a supersonic-exit solution the following plasma regions are identified: anode sheath (AB), anode presheath (BC), diffusion region (CD), ionization layer (DH), internal acceleration region (HE), near-plume (EP), and far-plume (P∞). Point B is a singular sonic point for the reverse ion flow and point S is a regular sonic point of the forward ion flow.

the anode to the quasineutral diffusion flow of electrons across the thruster channel. We consider that only neutral gas is supplied externally through the anode. Then, since the anode sheath is thin and ion-attracting, ions must flow *into* the sheath from the quasineutral region adjacent to the anode. The presence of a region with reverse ion flow between the anode and the ionization layer is well reported in Refs. 1 and 5. The reverse ion flow is recombined at the anode, and re-emitted as neutral gas to the channel, adding itself to the gas flow supplied externally.

Our macroscopic model considers that the plasma is composed by three independent fluids: electrons (e), ions (i), and neutrals (n), and formulates equations for particle, momentum, and energy conservation of the three species. The set of differential equations for the stationary response of the quasineutral plasma is

$$\frac{d}{dx}(An_e v_i)=\frac{d}{dx}(An_e v_e)=-\frac{d}{dx}(An_n v_n)=An_e\nu_i, \tag{2}$$

Downloaded 07 Jun 2001 to 138.4.73.144. Redistribution subject to AIP license or copyright, see http://ojps.aip.org/pop/popcr.jsp

$$v_n = \text{const}, \tag{3}$$

$$m_i v_i \frac{dv_i}{dx} = -e\frac{d\phi}{dx} - \nu_i m_i (v_i - v_n), \tag{4}$$

$$0 = e n_e \frac{d\phi}{dx} - \frac{d}{dx} n_e T_e - \nu_d m_e n_e v_e, \tag{5}$$

$$v_e \frac{d}{dx}\left(\frac{3}{2}T_e\right) = -T_e \frac{dv_e}{dx} + \nu_d m_e v_e^2 - \nu_i\left(\alpha_i E_i + \frac{3}{2}T_e\right). \tag{6}$$

Here m_α, n_α, and $v_\alpha (\alpha = i,e,n)$, are particle mass, particle density, and *axial* velocity, respectively; ϕ is the electric potential and e is the unit of electric charge (all ions are considered singly charged); T_e is the electron temperature (in energy units); E_i is the ionization energy of the gas ($E_i = 12.1$ eV for xenon) and α_i takes into account the effective energy loss per actual ionization, due to excitation collisions ($\alpha_i \sim 2-3$ according to Ref. 1); ν_i is the ionization frequency; and ν_d is the effective frequency for the electron axial diffusion. The ion temperature is expected to be smaller than the electron temperature; this allows one to neglect the ion pressure in Eq. (4) and to avoid the equation for the ion energy.

The present version of the model ignores the interaction of the plasma with lateral walls. This would consist of (i) recombination and secondary emission, (ii) thermal losses, and (iii) additional electron diffusion. These effects can be included in the 1-D axial model through *three* additional terms. A preliminary version for these terms was presented in Ref. 14 but we find it still requires further improvements.

The ionization frequency is expressed as

$$\nu_i = n_n R_i(T_e),$$

where $R_i(T_e)$ is the effective ionization rate per electron. The dependence of R_i on the electron temperature is going to be crucial in shaping the ionization region, so it is important to use a correct expression for it. In Appendix A we analyze the experimental data for the ionization cross-section and propose Eq. (A3) as a good approximation of $R_i(T_e)$ for T_e in the range of interest.

Equations (5) and (6) for the electron dynamics require some discussion. Those equations are based on the quasi-closed drift approximation, which requires us to satisfy

$$|\mathbf{v}_e| \ll \sqrt{T_e/m_e}, \tag{7}$$

$$\nu_e \ll \omega_e, \tag{8}$$

where $\omega_e = eB/m_e$ is the electron gyro-frequency, and ν_e is the total collision frequency for electron momentum. The first condition makes negligible the contribution of the convective terms to the momentum equation; as a consequence, the electron kinetic energy of mean motion is also negligible in the energy equation. Then, neglecting inertia terms in the azimuthal component of the momentum equation, Eq. (8) yields that the ratio between the azimuthal and axial velocities,

$$v_{e\theta}/v_e \simeq -\omega_e/\nu_e, \tag{9}$$

is very large. Substituting $v_{e\theta}$ from this equation into the axial component of the momentum equation, one obtains Eq. (5) with

$$\nu_d \simeq \omega_e^2/\nu_e. \tag{10}$$

Equation (6) for the electron internal energy includes the Joule heating due to the diffusion current and the ionization and excitation losses. For the Joule heating, using Eqs. (9) and (10), one has

$$m_e \nu_e |\mathbf{v}_e|^2 \simeq m_e \nu_e v_{e\theta}^2 \simeq m_e \nu_d v_e^2.$$

As a closure relation for the electron macroscopic equations, Eq. (6) assumes that the axial heat conduction q_e is negligible, which is valid as long as $q_e \ll T_e n_e v_e$.

The collision frequency for electrons is the sum of $e-i$ collisions, $e-n$ collisions, plus possible anomalous collision processes:

$$\nu_e = \nu_{ei} + \nu_{en} + \nu_{\text{ano}}.$$

For typical thruster conditions Coulomb collisions appear to be unimportant;[11] they will be neglected here. The electron–neutral collision frequency is expressed as

$$\nu_{en} = n_n \sigma_{\text{en}} \overline{c_e},$$

with $\overline{c_e} = \sqrt{8T_e/\pi m_e}$ the electron thermal velocity and $\sigma_{\text{en}} \simeq \text{const}$ in the range of interest ($\sigma_{\text{en}} \simeq 27 \times 10^{-20}\ \text{m}^2$ for Xe). Near the channel exhaust, where the neutral density is low, classical collisions, $\nu_{ei} + \nu_{en}$, are insufficient to explain the plasma behavior observed there, which suggests the presence of an anomalous collisionality. There is controversy about which is the phenomenon responsible for that collisionality. Some authors suggest electron exchanges at lateral walls,[11,17] but experimental data[9,18] seems to favor Bohm diffusion. We opted here for this last mechanism and took

$$\nu_{\text{ano}} = \alpha_{\text{B}} \omega_e,$$

with α_{B} the Bohm parameter ($\alpha_{\text{B}} \sim 1/16$ in the classical formulation).

Using the particle axial flows of the different species as $\Gamma_\alpha = A n_\alpha v_\alpha$, the mass flow and the discharge current are written as

$$\dot{m} = m_i \Gamma_m, \quad \Gamma_m = \Gamma_i + \Gamma_n,$$

$$I_d = e\Gamma_d, \quad \Gamma_d = \Gamma_i - \Gamma_e,$$

and continuity equations (2) show that these two magnitudes are constant along the plasma jet (except for Γ_d dropping abruptly to zero at the cathode). Notice that $\dot{m}$ includes only the gas flow delivered at the anode. Another useful equation, derived from Eqs. (2)–(6), is the ambipolar momentum equation

$$\frac{d}{dx}(A m_i n_e v_i^2) + A\frac{d}{dx}(n_e T_e) = A n_e (\nu_i m_i v_n - \nu_d m_e v_e). \tag{11}$$

Finally, important ratios for a discussion of the plasma response are (i) the ratio between the discharge current and the emitted gas flow,

Downloaded 07 Jun 2001 to 138.4.73.144. Redistribution subject to AIP license or copyright, see http://ojps.aip.org/pop/popcr.jsp

$$i_d = \frac{m_i I_d}{e\dot{m}} \equiv \frac{\Gamma_d}{\Gamma_m}, \tag{12}$$

and (ii) the local ion current fraction,

$$\eta_i(x) = \Gamma_i(x)/\Gamma_m. \tag{13}$$

The propellant utilization is defined as $\eta_u = \eta_{i\infty}$. For $i_d > 1$ (the usual case in practice) η_u can be near unity;[17] in this case, i_d^{-1} coincides with the electrical efficiency $\Gamma_{i\infty}/\Gamma_d$. However, for $i_d < 1$, the maximum propellant utilization can be just i_d.

A. Singular/sonic points

We discuss now the properties of the mathematical model. Explicit equations for the spatial derivatives of the variables are straightforward to obtain from Eqs. (2)–(6). It is then found that the spatial problem may present singular points where the Mach number,

$$M = \frac{v_i}{\sqrt{5T_e/3m_i}},$$

is equal to -1 or $+1$. For instance, the equation for the dn_e/dx is

$$Pv_e dn_e/dx = n_e G,$$

with $P = T_e - (3/5)m_i v_i^2$ and

$$G = \nu_i\left[\frac{2}{5}\alpha_i E_i + T_e - \frac{3}{5}m_i v_e(2v_i - v_n)\right] - \nu_d m_e v_e^2 + \frac{3}{5}m_i v_i^2 v_e \frac{d\ln A}{dx}. \tag{14}$$

The definition of an ion Mach number is *natural* to the macroscopic approach adopted to describe plasma dynamics. It characterizes the propagation of pressure perturbations, and clarifies, therefore, the interpretation of the steady and unsteady plasma responses.

Sonic points are *regular* or *singular* depending on G being equal or not to zero at them. In a *singular sonic point* the derivatives of all plasma variables become infinite, so it is a turning point of spatial profiles. These points are admissible only at the boundaries of the quasineutral channel. On the contrary, in *a regular sonic point* the ion flow changes smoothly from subsonic to supersonic, like in the classical problem of a convergent–divergent nozzle. The expansion of the ion beam from the channel into the rarefied ionosphere implies that the ion flow will be sonic or supersonic at the channel exit (point E). Therefore, a forward sonic point—point S in Fig. 1(b)—with $M_S = 1$ is always expected in the channel. For a choked exit, point S is singular and coincides with point E. For a supersonic exit, point S is regular and its position within the channel must be determined as part of the solution.

B. Plume divergence law

Inside the channel, the radial area of the plasma jet, $A(x)$, is constant and drops off from Eqs. (2)–(6). A law for dA/dx is needed to complete these equations in the external plume. For a cylindrical plasma flow, the area variation in the plume ($L < x$) verifies

$$\frac{d}{dx}\ln A = \frac{d}{dx}\ln h = \frac{2}{h}\tan\delta, \tag{15}$$

with $h(x)$ the radial thickness of the plume and δ the semiangle of divergence.

The simplest approximation[12] would be to assume $\delta = \text{const}$. Instead, experimental measurements by Pollard and Beiting[19] indicate that what remains practically constant (in the near plume) is the radial velocity of expansion of the plume boundaries. Based on this, we assume that the plume boundary lines expand radially with the sound velocity at the thruster exhaust, which implies that we take

$$\tan\delta = \frac{\sqrt{5T_{eE}/3m_i}}{v_i}. \tag{16}$$

It is plausible that this 1-D model of the plume will be more correct for supersonic-exit solutions than for choked-exit solutions because the divergence is presumably smaller. Besides, we expect the model to be correct only in the near plume; the far plume is just included in the paper to estimate in Sec. IV A the thrust and the thrust efficiency.

C. Anode sheath

The Debye sheath attached to the anode (region AB in Fig. 1) completes the 1-D model of the channel and defines two boundary conditions at point B for the quasineutral model. The sheath is needed to assure the continuity of the electric current from the channel to the anode. A space-charge field adjusts the potential jump in the sheath, $\phi_{\text{sh}} \equiv \phi_B - \phi_A$, to a value such that the flow of electrons reaching the anode is equal to the diffusive flow $|\Gamma_{eB}|$ coming from the quasineutral channel. Assuming a quasi-Maxwellian distribution of electrons the potential jump satisfies

$$\frac{e\phi_{\text{sh}}}{T_{eB}} = \ln\frac{\overline{c}_{eB}}{4|v_{eB}|}, \tag{17}$$

with $\overline{c}_{eB}$ the thermal velocity at B.

It is well known that the transition from a quasineutral plasma to a Debye sheath requires the plasma flow to meet the Bohm condition at point B. A two-scale analysis of our macroscopic model plus the Poisson equation shows that the Bohm condition states that $-M_B \geqslant 1$. Were $-M_B > 1$, there would be a point within the channel with $M = -1$ and $G = 0$, which is not possible, as the solution will make evident. Therefore, point B must be a singular point for the quasineutral, reverse flow:

$$M_B = -1. \tag{18}$$

Using this relation in Eq. (17), one has

$$\frac{e\phi_{\text{sh}}}{T_{eB}} = \ln\left(\frac{\Gamma_{iB}}{\Gamma_{eB}}\sqrt{\frac{3m_i}{10\pi m_e}}\right), \tag{19}$$

Downloaded 07 Jun 2001 to 138.4.73.144. Redistribution subject to AIP license or copyright, see http://ojps.aip.org/pop/popcr.jsp

where the variable under the logarithm must be large to be consistent with the diffusive-motion hypothesis, Eq. (7). This means $|\Gamma_{iB}|/\Gamma_d$ should be larger than 1%, roughly.

Finally, we point out that a 1-D model of the sheath and the region around it is an idealized situation, since, in general, the gas is ejected from a small orifice into the channel, yielding a two-dimensional potential distribution.

D. Boundary conditions

The integration of Eqs. (2)–(6) between points B and P require seven boundary conditions, which are distributed between points B and S, E, and P^-. Taking into consideration the model characteristics discussed until here and the parameters that can be controlled experimentally, a *natural* set of boundary conditions is the following.

(i)–(ii) The externally supplied mass flow rate $\dot{m}$ and the neutral velocity v_{nA} are known.

(iii) The electron temperature at the cathode, T_{eP} (of the order of the electron emission temperature) is known.

(iv) The discharge voltage $V_d=\phi_A-\phi_P$ is known.

(v) The voltage difference at the sheath satisfies Eq. (19). (Placing the arbitrary origin of ϕ at point A, one has $\phi_B=\phi_{\rm sh}$ and $\phi_P=-V_d$.)

(vi) Bohm condition (18) is satisfied at the sheath transition.

(vii) For the *supersonic exit regime*, sonic point S is regular:

$$G_S=0, \quad \text{at} \quad M_S=1. \tag{20}$$

Instead, for the *choked exit regime* we set that the flow at point E is sonic:

$$M_E=1.$$

Apart from V_d, $\dot{m}$, and T_{eP}, other input variables are v_{nA}, L, L_{EP}, A_c, and the profile of the magnetic field, Eq. (1). The main output variables of the model are the discharge current I_d, the relative ion reverse flow η_{iB}, the position x_S of the sonic point S (for a supersonic exit), the plume divergence profile, the thrust, and the thrust efficiency.

The continuation of the solution from point P to ∞ is straightforward. It just requires us to modify the electron current at point P^+, setting $\Gamma^+_{eP}=\Gamma_{iP}$, in order that the net electric current in the plume far-field be zero.

III. TYPES OF SOLUTIONS

It is convenient to use dimensionless variables and parameters to integrate the equations and to characterize the solutions. Three magnitudes are enough to nondimensionalize Eqs. (2)–(6). The energy $T_*=E_i$, the cross-section $\sigma_*=\sigma_{i0}(m_i/m_e)^{1/2}$, and a typical particle flow Γ_* are the best choice. Then, magnitudes related to these three are

$$v_*=\sqrt{T_*/m_i}, \quad n_*=\Gamma_*/A_c v_*, \quad l_*=1/n_*\sigma_*,$$

$$\nu_*=v_*/l_*.$$

When necessary, dimensionless magnitudes will be represented by an overtilde over the respective dimensional ones. We omit to write down the dimensionless form of plasma equations, which is immediate.

The dimensionless form of Eqs. (2)–(6) is integrated as an initial-value problem with a Runge–Kutta algorithm. We focus the discussion here in the region between points B and P, the continuation to the far-plume being straightforward. The use of the auxiliary variable ξ, defined by

$$dx/d\xi=P,$$

instead of x, avoids unnecessary numerical problems in reaching or departing from singular sonic points, like point B. However, this does not solve the crossing of regular sonic point S in the supersonic-exit regime. A Taylor expansion of Eqs. (2)–(6) is needed to determine the derivatives of the plasma variables there; the details of that expansion are omitted here.

Due to the character of point S, the less time-consuming procedure is clearly to integrate from the neighborhood of point S towards points B and P separately. At point B, the integration stops where condition $M_B=-1$ is reached; at point P, it ends where $T=T_{EP}$. This initial-value procedure requires setting all variables at point S. For the choked-exit regime, this implies taking output parameters η_{iS}, i_d, and $\tilde{T}_{eS}$ as initial parameters, while input parameters $\tilde{V}_d$, $\tilde{x}_A$, and $\tilde{x}_P$ are outputs of the integration. For the supersonic-exit regime, output parameters i_d, η_{iS}, and $\tilde{x}_S$ are used as initial parameters, and $\tilde{T}_{eS}$ comes from condition $G_S=0$; as before, input parameters $\tilde{V}_d$, $\tilde{x}_A$, and $\tilde{x}_P$ are outputs of the integration. A subsequent iteration is needed to adjust these input parameters to their desired values.

In addition, not all sets of ''initial parameters'' lead to valid solutions. A first restriction to these parameters comes from the condition that the plasma flow be accelerating at point S: $dv_i/dx|_S>0$. For a supersonic-exit solution this means choosing the appropriate set of derivatives from the two solutions given by the Taylor expansion. For a choked-exit solution it reduces the region of valid parameters to those satisfying

$$G_S^->0 \quad \text{and} \quad G_S^+<0; \tag{21}$$

observe in Eq. (14) that the difference between G_S^+ and G_S^- is due to the term containing $d\ln A/dx\propto(\tan\delta)/h$.

A second restriction to ''initial parameters'' at point S comes from the fact that there are solutions departing from S^- towards B, which never reach a negative ion velocity and finish instead in a singular point with $M=+1$. These solutions are disregarded since they have no physical meaning for the plasma in a conventional Hall thruster. The limit condition $\Gamma_{iB}\simeq 0$ is going to be very important since it is going to indicate a real physical condition for the disappearance of steady solutions.

Figure 2 illustrates, in the parametric plane $(\tilde{T}_{eS},\eta_{iS})$ and for two values of i_d, Eq. (12), the different solutions that are obtained from the integration between points S and B. Four parametric regions are found: *region 1*, with $G_S^-<0$, and *region 2*, with $G_S^->0$ and $\eta_{iB}>0$, are forbidden regions

Downloaded 07 Jun 2001 to 138.4.73.144. Redistribution subject to AIP license or copyright, see http://ojps.aip.org/pop/popcr.jsp

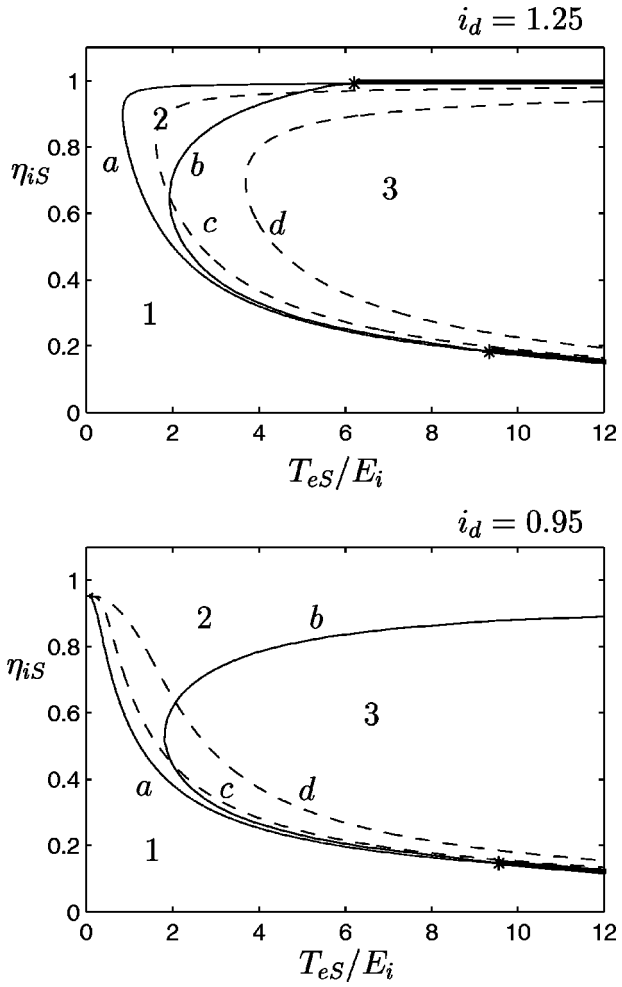

FIG. 2. Regions leading to different types of solutions between points S and B for two values of i_d and a constant B-profile. Line *a* corresponds to $G_S^- = 0$; line *b* to $\eta_{iB} \to 0$; lines *c* and *d* to $G_S^+ = 0$ for $\tilde{h}/\tan\delta = 0.3$ and 0.1, respectively. Region 2 is between lines *a* and *b*; region 4 (supersonic-exit regime) corresponds to the thick parts of line *a*, to the right of the intersections (asterisks) with line *b*. Some parameter values are $\Gamma_* = \Gamma_m$, $\omega_e/\nu_* = 84.6\sqrt{m_i/m_e}$, $\tilde{v}_{nA} = 0.1$, $\alpha_i = 2.5$, and $\alpha_B = 1/80$.

for the reasons exposed above; *region 3*, with $G_S^- > 0$ and $\eta_{iB} < 0$, corresponds to the *choked-exit regime*; and (line) *region 4*, with $G_S = 0$ and $\eta_{iB} < 0$, corresponds to the *supersonic-exit regime*. For the choked-exit regime, the continuity of the solutions into the plume requires that $G_S^+ < 0$, Eq. (21). Figure 2 depicts the limit line $G_S^+ = 0$ for two values of $(\tan\delta)/\tilde{h}$.

For $i_d = 1.25$, region 4 of supersonic-exit solutions consists of high and low ionization branches. The low-ionization branch yields propellant utilizations well below 50% and corresponds, then, to inefficient thruster operation. Since, in addition, it does not lead to different plasma dynamics than the high-ionization branch, it will be disregarded hereafter in this paper. The high-ionization branch is actually a near-total ionization branch and corresponds to the near-complete ionization mode referred by Morozov *et al.*[17] Notice that, since $\eta_{iS} \simeq 1$, point S must be placed near the downstream end of the ionization layer (point H in Fig. 1). As i_d increases from 1.25, the line $\eta_{iB} \simeq 0$ (separating regions 3 and 4 from region 2) moves left, towards lower T_{eS}, and region 2 disappears eventually (at $i_d \sim 1.65$ for the case of Fig. 2). For the same reason, as i_d decreases from 1.25 the line $\eta_{iB} \simeq 0$ moves right and restricts, in particular, the domain of supersonic-exit solutions with large ionization. For $i_d \leqslant 1$, two features are to be pointed out: first, the high-ionization branch of the supersonic-exit regime, instead of approaching the asymptotic line $\Gamma_{iS} = \Gamma_d$ (i.e., $\eta_{iS} = i_d$), disappears; second, the line $\eta_{iB} \simeq 0$ forbids choked-exit solutions with large ionization and moderate temperatures.

The presence and characteristics of the two supersonic-exit branches can be explained from the analytical expression of $G_S = 0$. From Eq. (14), that condition yields

$$\frac{3\Gamma_{iS}}{5\Gamma_m}(\Gamma_m - \Gamma_{iS})\,\frac{(2\Gamma_d - \Gamma_{iS})T_{eS} + (2/5)\Gamma_{iS}\alpha_i E_i}{T_{eS}(\Gamma_d - \Gamma_{iS})^2} \simeq \frac{\overline{\nu}_{dS}}{\nu_i^*}, \tag{22}$$

with $\overline{\nu}_d = \nu_d m_e/m_i$ and $\nu_i^* = n_{nA} R_i(T_{eS})$, and this last magnitude is of the order of the maximum ionization frequency in the channel. Then, for plasmas satisfying

$$\overline{\nu}_{dS} \ll \nu_i^*, \tag{23}$$

it is readily seen that Eq. (22) is verified by two types of solutions: the low-ionization branch with $\Gamma_{iS} \ll \Gamma_m$; and the near-total ionization branch with $\Gamma_{iS} \simeq \Gamma_m$, which exists only for $\Gamma_d > \Gamma_m$.

In conclusion, we have shown that a *regular* sonic point (with no discontinuity in plasma derivatives) may exist inside a channel of constant area in a *natural* way by compensation of diffusion and ionization effects. This implies that the sonic point is within or close to the ionization layer. The position of the sonic point is not set *a priori*, it depends on the control parameters and is part of the solution of the problem. Regular sonic transitions were also discussed by Fruchtman and Fisch.[10] In addition, they suggested forcing a choked internal point by introducing a current discontinuity; thus, their solution matches two choked flows (with $G_S^- > 0, G_S^+ < 0$) at the prescribed discontinuity point.

IV. STRUCTURE OF THE PLASMA FLOW

The preceding section has shown that supersonic-exit solutions with i_d moderately above 1 seems to be the most efficient operating regime of a Hall thruster. The results we show next on the plasma structure and the thruster output parameters will confirm this. These results are presented in dimensional form to facilitate the comparison with real experiments.

Figures 3(a)–3(i) show spatial profiles of the main plasma variables for a supersonic-exit solution and geometrical and operational parameters typical of a SPT-100 thruster;[6] all parameters are listed in the figure caption. We observe that the structure of the plasma response can be divided into the six regions sketched in Fig. 1(b). The first significant feature is that the *ionization region* is placed in the middle of the channel, more or less between points D and H, which can be defined as the places where v_i changes sign and T_e is maximum, respectively; this yields $x_D \sim 13.6$ mm and $x_H \simeq 17.4$ mm, with $T_{eH} \sim 91.3$ eV. Notice in Fig. 3(b)

Downloaded 07 Jun 2001 to 138.4.73.144. Redistribution subject to AIP license or copyright, see http://ojps.aip.org/pop/popcr.jsp

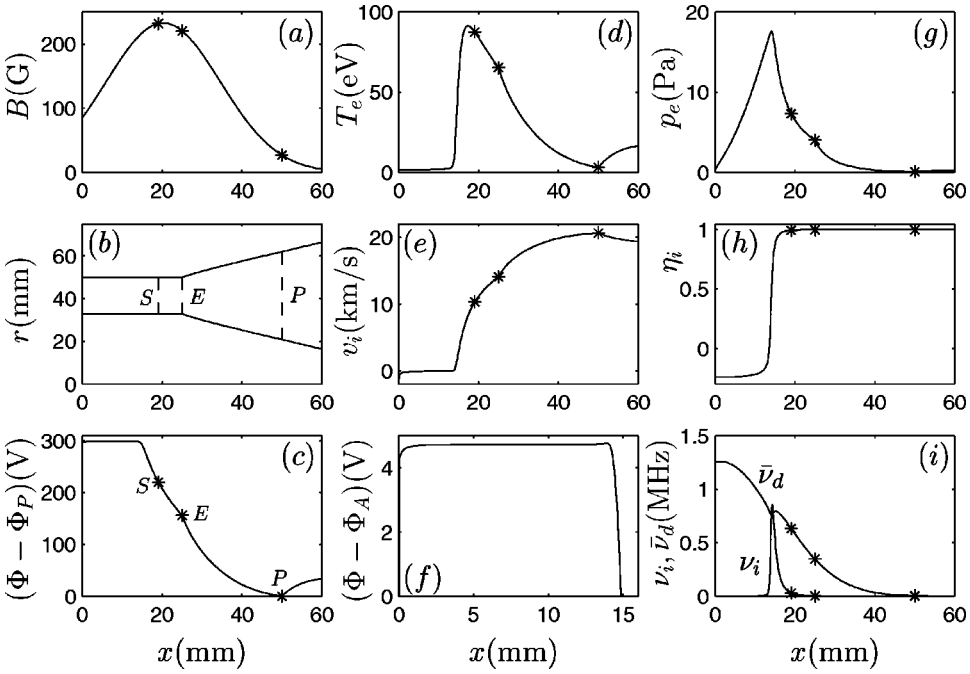

FIG. 3. Supersonic-exit solution for xenon, $B(x)$ as shown in (a) ($B_m \simeq 233$ G, $x_m \simeq 20.3$ mm, $L_m \simeq 20.2$ mm), the channel geometry shown in (b) ($L \simeq 25$ mm, $h_c \simeq 17.2$ mm, $A_c \simeq 45$ cm^2, $L_{EP} \simeq 25$ mm), $\dot{m} \simeq 5.32$ mg/s, $V_d \simeq 293.3$ V, $T_{eP} \simeq 2.7$ eV, $v_n \simeq 300$ m/s, and $\alpha_B \simeq 1/80$. The profile of the plume in (b) is part of the solution; subplot (f) is a magnified copy of subplot(c) for region AS; asterisks represent points S, E, and P; and $\bar{\nu}_d \equiv (m_e/m_i)\nu_d$ in (i).

the peaked shape of $\nu_i(x)$. The point of maximum electron pressure, $p_e = n_e T_e$, is at $x \simeq 14.1$ mm, very near to the proposed entrance of the ionization layer. The sonic point S is downstream of point H ($x_S \simeq 19$ mm) and the temperature there ($T_{eS} \simeq 89.6$ eV) is close to the peak temperature; notice that point S cannot be far from point H since the ionization terms are needed to define the crossing condition $G_S = 0$, Eq. (22).

Upstream of the ionization layer is the large *diffusion region* (region CD), characterized by a reverse, low-velocity ion flow, a low electron temperature (~ 2 eV), an insignificant electric field ($\phi_C - \phi_D \sim 1$ V) and a quasi-linear pressure gradient as the force driving the electron diffusion. The relative value of the reverse ion flow is $|\eta_{iB}| \simeq 0.24$ (of the order of the one measured in Ref. 1). Tied to the anode, there is the *anode sheath* (region AB) characterized by a potential jump $\phi_{\rm sh} \simeq 3.8$ V and a negligible thickness in the channel scale ($x_B \simeq x_A = 0$ for $\lambda_D/L \to 0$.). The *anode presheath* (region BC) is a transition region between the sheath and the diffusion region, where the reverse ion flow is accelerated to meet the Bohm condition at the sheath entrance; it is rather thin ($x_C - x_B \sim 1$ mm) and observable in Fig. 3(f) only.

The sharp transition from the diffusion region to the ionization region is related to the exponential dependence of the ionization cross-section on the electron temperature T_e, as we will further comment on below. The large value of T_e in the ionization region—and its low value in the diffusion region—are consequences of excluding the heat conduction and the losses to lateral walls. The electric potential remains practically constant until well inside the ionization layer, then it starts decreasing; the total potential variation across the ionization layer is $\phi_D - \phi_H \simeq 51.4$ V.

Downstream of the ionization layer there is the *internal acceleration region* (region HE), where the ion flow is accelerated by the electric field. The potential decrement in this region is $\phi_H - \phi_E \simeq 91.0$ eV and the temperature at the channel exhaust is still large ($T_{eE} \simeq 65.3$ eV) so the effects of the electron pressure are significant there still. The *plume* is the extension of the internal acceleration region. The form of the plume profile shown in Fig. 3(b) comes from the solution of Eq. (15). The semi-angle of divergence is maximum at the channel exit, $\delta_E \simeq 32.3°$, but it does not change much since most of the increase of the ion velocity took place inside the channel; the typical range of δ in experiments[20,21] is $30° - 40°$. In the near-plume (region EP) the radial area increases from $A_E = A_c \simeq 45$ cm^2 to $A_P \simeq 76$ cm^2. The potential variation in the near-plume is $\phi_E - \phi_P \simeq 150$ V, about 53% of the total discharge voltage. The minimum of the electric potential at the cathode (point P) provides the electric field required to move the electrons into the beam. Indeed, the potential variation in the far-plume, $\phi_\infty - \phi_P \simeq 34.8$ V, can be considered as a part of the energy loss associated to the cathode.

There are two ''free'' parameters in the solution of Fig. 3: L_{EP} and α_B. The first parameter seems to affect weakly the plasma response except when it becomes too small. On the contrary, the plasma response is very dependent on the value of the Bohm parameter. In fact, the best fit with experimental results is obtained with $\alpha_{\rm B} \sim 1/80$ instead of the classical value, $\alpha_{\rm B} = 1/16$. For the chosen value of $\alpha_{\rm B}$ anomalous diffusion becomes dominant only downstream the ionization region, as the quick change in the derivative of ν_d around point D, in Fig. 3(i), illustrates.

The plasma structure for a choked-exit solution is very similar to the one presented here except that (i) ionization might not be near-total, (ii) the region of supersonic acceleration is totally external, and (iii) the plume divergence is large. Indeed for practical values of h/L, the condition $G_S^+ = 0$, depicted in Fig. 2, leads to divergence angles above 45°, larger even than those given by Eq. (16). Clearly, the 1-D plume model is hard to apply there. This consideration

Downloaded 07 Jun 2001 to 138.4.73.144. Redistribution subject to AIP license or copyright, see http://ojps.aip.org/pop/popcr.jsp

and the fact that the experimental data fit in general well with supersonic-exit solutions makes advisable to continue the investigation of choked-exit solutions.

A. Thruster performances

Looking again at the case of Fig. 3, we show now that the main output parameters for thruster performances agree rather well with experimental values.[6] The discharge current is $I_d \simeq 4.36\,\mathrm{A}$ (versus 4.5 A experimentally.) The thrust, computed at the channel exhaust as

$$F = m_i(\Gamma_i v_i)_E + (p_E - p_\infty)A_c,$$

is $F \simeq 92.8\,\mathrm{mN}$ (versus 82 mN experimentally). The thrust efficiency, defined in the usual way as

$$\eta = F^2/2\dot{m} I_d V_d,$$

is $\eta \simeq 63\%$ (versus 52% experimentally, excluding cathode flow). Energy losses neglected in this model will reduce somehow these two last magnitudes. It is interesting to measure how different phenomena affect the thrust efficiency. This can be factorized as

$$\eta = \eta_u^2 \eta_e \eta_p / i_d,$$

with $\eta_u = \eta_{i\infty}$ the propellant utilization, Eq. (13), $\eta_e = m_i v_{i\infty}^2/2eV_\infty$ the energy efficiency, and $\eta_p \equiv \eta_{pc}\eta_{pd}$ the plume efficiency, this last one split into the cathode efficiency: $\eta_{pc} = V_\infty / V_d$, and the divergence efficiency: $\eta_{pd} = F^2/F_\infty^2$, with $F_\infty = m_i(\Gamma_i v_i)_\infty$. For the case of Fig. 3, one has, first, that the propellant utilization and the energy conversion are practically total: $\eta_u \simeq 100\%$, and $\eta_e \simeq 99.3\%$. Efficiency losses are distributed among the other three contributions: $i_d^{-1} \simeq 88.7\%$, $\eta_{pc} \simeq 88.1\%$, and $\eta_{pd} \simeq 81.1\%$.

The present model does not consider the gas spent in the cathode for electron emission, which amounts to a 5–10% of the total gas flow, typically,[20] and most of it (above 90%) is ejected into the plume without ionizing. On the one hand, this gas flow contributes as a loss to the thruster efficiency; on the other hand it is responsible for charge-exchange and backflow effects in the plume.

V. ASYMPTOTIC ANALYSIS

We derive here approximate solutions for the different plasma regions that explain most of the features observed in the exact solution studied in the preceding section.

Since ionization is limited to a thin layer, the zero-ionization form of the plasma equations will be applicable to most of the plasma flow. Making $\nu_i \to 0$ in Eqs. (2)–(5), one has conservation equations for particles, ion energy, and electron enthalpy,

$$\Gamma_\alpha = \text{const} \quad (\alpha = i, e, n), \tag{24}$$

$$m_i v_i^2/2 + e\phi = \text{const}, \tag{25}$$

$$5T_e/2 - e\phi = \text{const}. \tag{26}$$

To avoid integral terms with the electron diffusion frequency and simplify thus the analytical expressions, we will use, instead of a continuous function, two constant (i.e., average) values: $\nu_d = \nu_{d0}$, for the whole back-flow region AD, and $\nu_d = \nu_{d1}$, for the whole acceleration region DP.

We proceed to integrate Eqs. (2)–(6) from point B (with $x_B \simeq x_A = 0$, $M_B = -1$) towards the cathode P. To neglect ionization in the rear part of the channel we assume that $T_{eB} \ll E_i$. Then, from Eqs. (24)–(26) and (11) the ion velocity satisfies

$$\frac{v_i}{v_{iB}} = \frac{n_{eB}}{n_e} \simeq 1 + \frac{x}{x_C} - \sqrt{\left(1 + \frac{x}{x_C}\right)^2 - 1}, \tag{27}$$

where $v_{iB} = -\sqrt{5T_e/3m_i}$ and

$$x_C = \frac{8}{5}\frac{m_i |v_{iB}|}{m_e \nu_{d0}}\frac{\Gamma_{iB}}{\Gamma_{eB}}$$

is the characteristic thickness of the anode presheath. Observe that x_C tends to zero with Γ_{iB}.

The *diffusion region* corresponds to $x \gg x_C$. From Eq. (27), the asymptotic behavior of the ion velocity is

$$v_i / v_{iB} \simeq x_C/2x \to 0.$$

The plasma temperature and the voltage also tend to constant values,

$$T_e \to T_{eC} = (4/3)T_{eB}, \quad e\phi \to e\phi_C = e\phi_B + (5/6)T_{eB}, \tag{28}$$

so the electric field tends to zero. On the contrary, the electron pressure increases monotonically:

$$p_e \simeq p_{eB} + |\Gamma_e / A_c| m_e \nu_{d0} x, \tag{29}$$

and provides the driving force for the electron axial motion in the diffusion region. Since $T_e \simeq \text{const}$, the plasma density changes in the same way as the pressure. Weak electric fields and nonzero density gradients upstream of the ionization layer are confirmed by experiments.[1]

The *transition to the ionization region* (around point D) requires the inclusion of small ionization effects. The evolution of T_e there is governed by the exponential dependence of the ionization rate on T_e, for $T_e/E_i \ll 1$. Keeping $d\phi/dx \simeq 0$ and using Eq. (29) for p_e, the electron temperature in this transition layer satisfies

$$\frac{dT_e}{R_i(T_e)} \simeq -n_n \frac{T_e + \bar{\alpha}_i E_i}{T_e} m_e \nu_{d0} x dx$$

($\bar{\alpha}_i = 2\alpha_i/5$), and its approximate solution is

$$x^2 \simeq L_{AD}^2 - \frac{2T_e^3}{(T_e + \bar{\alpha}_i E_i) E_i m_e \nu_{d0} n_n R_i(T_e)}, \tag{30}$$

with

$$L_{AD}^2 \simeq \frac{2T_{eC}^2}{\bar{\alpha}_i E_i^2} \times \frac{T_{eC}}{m_e \nu_{d0} \nu_{iC}}. \tag{31}$$

Equation (30) yields $T_e(x)$ implicitly, showing a large gradient around $T_e/E_i = O(1)$, where the ionization rate $R_i(T_e)$ increases sharply. This justifies that L_{AD}, as defined by the two last equations, is effectively the length of region AD. Equation (31) shows also how the position of the ionization layer is influenced by different factors. The pressure satisfies Eq. (29) up to the ionization layer and, setting its maximum around point D, one has

Downloaded 07 Jun 2001 to 138.4.73.144. Redistribution subject to AIP license or copyright, see http://ojps.aip.org/pop/popcr.jsp

$$p_{eD} \simeq |\Gamma_{eB}/A_c| m_e \nu_{d0} L_{AD}. \tag{32}$$

The plasma density, obtained from p_e/T_e, gets its maximum before point D, due to the fast increase of T_e.

A complete analytical solution for the *ionization layer* is not available, but there are several useful expressions relating point D and point S (just downstream of point H, as we commented on previously). Conditions $v_n/v_{iS} \ll 1$ and (23) are enough, generally, to neglect electron diffusion in the bulk of the ionization layer, and the right-hand side of the ambipolar momentum equation (11). Then, one has

$$m_i n_e v_i^2 + p_e \simeq p_{eD},$$

across that layer. Particularizing at point S and using $M_S = 1$ we obtain two relations:

$$p_{eS} = \frac{3}{8} p_{eD}, \quad T_{eS} = \frac{5 p_{eS}^2 A_c^2}{3 m_i \Gamma_{iS}^2}, \tag{33}$$

and $\Gamma_{iS} \simeq \Gamma_m$ for a supersonic-exit solution. From Eqs. (2) and (32), the estimated thickness of the ionization layer is

$$L_{DH} \sim L_{DS} \sim \frac{v_{iS}}{\nu_i^*} \sim \frac{m_e \nu_{d0}}{m_i \nu_i^*} L_{AD},$$

and $L_{DS} \ll L_{AD}$, as expected. From Eq. (4), the potential jump across the ionization layer is

$$e\phi_D - e\phi_S \simeq \frac{5}{6} T_{eS} + m_i \int_{x_D}^{x_S} v_i \nu_i dx \equiv (1+\delta_i) \frac{5}{6} T_{eS}, \tag{34}$$

with parameter δ_i small (~ 0.10) in the cases we have analyzed.

In the *acceleration region* and the *plume* of a supersonic-exit solution, there are practically no neutrals to ionize and Eqs. (24)–(26) are applicable again. For $T_{eP} \ll T_{eS}$ and $\eta_{iS} \simeq 1$ one finds

$$v_{iP} \simeq 2 v_{iS}, \quad e\phi_S - e\phi_P \simeq (5/2) T_{eS}. \tag{35}$$

The area variation in the plume frustrates an exact integration of Eq. (11). Nevertheless, an approximate integration, useful to evaluate the influence of different parameters, is

$$p_{eS} \simeq \frac{3(\Gamma_d - \Gamma_m)}{2\overline{A}} m_e \nu_{d1} L_{SP},$$

with $\overline{A}$ an average value of the the radial area of the jet.

This completes the analysis on the different plasma regions. Adding the potential jumps in the different regions [Eqs. (28), (34), and (35)], one has

$$eV_d + e\phi_{\rm sh} \simeq \frac{5}{6} T_{eB} + \frac{20 + 5\delta_i}{6} T_{eS}.$$

Keeping only dominant terms, the maximum plasma temperature turns to be proportional to the discharge voltage,

$$T_{eH} \sim T_{eS} \simeq (3/10) e V_d.$$

This law agrees well with the numerical results of Fig. 3, which indicates that the overestimate of the maximum temperature is intrinsic to the present model. Therefore, energy losses at lateral walls and heat diffusion cannot be excluded in order to estimate correctly the plasma temperature.

VI. DISCUSSION

The preceding analysis has shown that the 1-D, macroscopic model we propose reproduces correctly the whole structure of the plasma in a Hall thruster: diffusion region, ionization layer, acceleration region, and near-plume. Although the main objective of the model was to understand the plasma behavior in the thruster, quantitative results for output parameters like thrust, efficiency, and discharge current agree well with experimental cases, which adds reliability to the model.

Attention has been paid to identifying the main phenomena that control the plasma response. We summarize the main aspects here, since previous models omit one or another. First, there is the dependence of the ionization rate on the electron temperature: the strong gradient of $R_i(T_e)$ around the ionization energy separates rather sharply the ionization and acceleration regions from the diffusion region and leaves this last region with a low temperature. Second, we have shown that a reverse ion flow is forced by physical conditions around the anode: solutions with $v_i \geqslant 0$ at the anode boundary are not compatible with an ion-attracting sheath and therefore do not satisfy the condition of current continuity there. Since the ionization layer starts around $v_i = 0$, the slow reverse ion flow is necessary to sustain the long diffusion region, also. The third and main aspect to emphasize is the crucial role of the electron pressure in all plasma regions: (i) the pressure term explains the subsonic to supersonic transition of the ion beam; (ii) the electron pressure is the only driving force for the electrons in the diffusion region, where the electric field is practically zero; (iii) the pressure drop, instead of the diffusion losses, balances the gain in ion momentum in the ionization layer; (iv) the maximum pressure is a central parameter controlling the position of the ionization layer.

Boeuf and Garrigues,[11] in spite of neglecting the electron pressure, recovers a zero-electric field upstream the ionization region, by making the B-field (and, therefore, the diffusion frequency) negligible there. From our preceding conclusions we find their solution debatable on the following grounds: (i) such a small B-field, which does not correspond to usual settings, violates the closed-drift condition sustaining the diffusive model of the electrons; (ii) they neglect the pressure term in the momentum equation in spite of being much larger than the electrostatic force; and (iii) the compression work is kept, however, in the energy equation.

The existence of a *regular* sonic point inside the thruster is not just a mathematical artifice. Physically, it implies the local balance between Ohmic heat dissipation into the electron gas and heat removal from it by ionization. The latter effect is strongly dominant near the ionization peak, whereas dissipation, although weaker, dominates outside the layer. Hence, the sonic balance can only be struck at a point where ionization has nearly ended or has just barely started. The second option is precluded by the fact that there is no mechanism ahead of the ionization layer that would provide the

Downloaded 07 Jun 2001 to 138.4.73.144. Redistribution subject to AIP license or copyright, see http://ojps.aip.org/pop/popcr.jsp

potential drop to accelerate the ions to their forward speed of sound. There is an interesting analogy between this ionization layer and the shock/combustion layer in a strong detonation front. In both cases, the downstream exit point of the layer is found to be sonic, although, of course, the layer inlet is supersonic in a detonation and subsonic in the ionization layer. The underlying mechanism is the same in both problems, the condition of a smooth sonic passage here being equivalent to the Chapman–Jouguet condition in combustion fronts, which states the local balance between the chemical heating and the heat diffusion. One interesting conclusion, valid for both, detonation and ionization layers, is that the occurrence of this ''Chapman–Jouguet condition'' is a consequence of the smallness of the ratio of two kinetic rates, and will only be as precise as this ratio is small.

A relevant conclusion, not fully investigated here, is that the presence of a reverse ion flow seems essential for the existence of stationary solutions, the zero-reverse flow condition indicating the transition to some nonstationary type of solutions. An almost finished parametric investigation on the effects of the main design parameters (discharge voltage, magnetic field, channel length, mass flow, ...) on the thruster performance indicates, for instance, that the excessive magnetic field eventually suppress the reverse ion flow and make it impossible to maintain steady-state quasineutrality in the diffusion region, in agreement with testing experience. Other important aspects that we are trying to clarify with this investigation are (i) how the position of the ionization layer inside the channel depends on the location of the maximum magnetic field and other parameters; and (ii) whether the transition from the complete to the incomplete ionization modes[17] corresponds to the transition from the supersonic-exit to the choked-exit solutions, or, on the contrary, from the high- to the low-ionization branches of supersonic exits.

The main flaw of the present model is the extremely high peak temperature. Effort is now being dedicated to modify the electron energy balance by including the plasma interaction with lateral walls and the heat conduction. For the first case, we are improving the radial model presented in Ref. 14. For the second case, the full analysis must be redone since the introduction of a second derivative of the electron temperature modifies substantially the mathematical formulation.

Finally, our semi-analytical model is very adequate to study the nature of plasma self-oscillations. Work is in progress to complete the analysis of the linearly-unsteady response initiated in Refs. 15 and 16.

ACKNOWLEDGMENTS

The work at E.T.S.I. Aeronáuticos (Madrid) was partially supported by the Dirección General de Enseñanza Superior e Investigación Científica of Spain, under Project No. PB97-0574-C04-02, and by the European Office for Aerospace Research and Development, under Contract No. F61775-00-WE034.

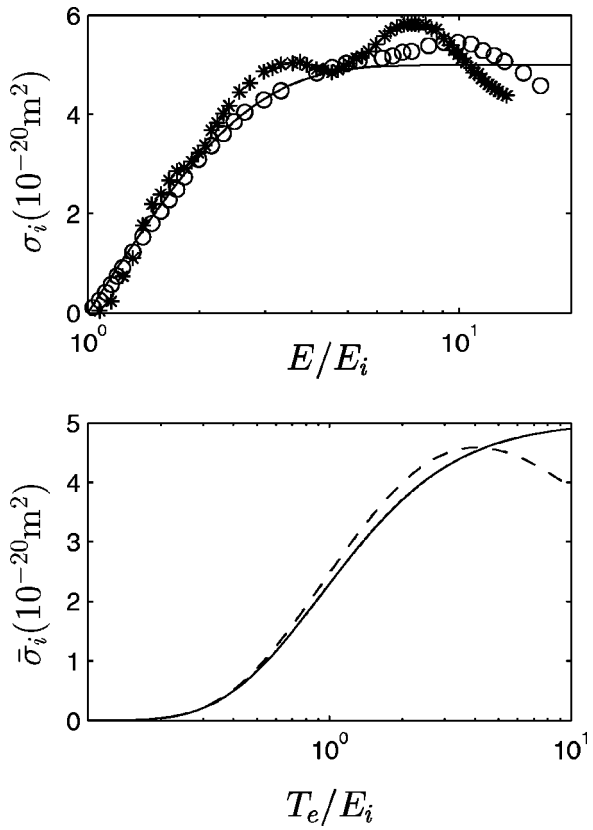

FIG. 4. Individual (σ_i) and collective ($\overline{\sigma_i}$) cross-section for single-ionization of xenon by electron impact; E is the energy of an individual electron and T_e is the temperature of the Maxwellian electron distribution. Asterisks and circles are experimental values taken from Refs. 22 and 23, respectively. The dashed line for $\overline{\sigma_i}$ corresponds to the integration of the (average) experimental points of $\sigma_i(E)$. Solid lines represent the analytical fittings given by Eqs. (A2) and (A3) for $\sigma_{i0}=5\times10^{-20}\,\mathrm{m}^2$.

APPENDIX: THE IONIZATION RATE

Here we look for an analytical expression of the ionization rate that reproduces correctly enough its dependence with the electron temperature. Since the electron motion is diffusive and verifies condition (7), the electron distribution function can be assumed locally Maxwellian,

$$f_e(E)=(m_e/2\pi T_e)^{3/2}\exp(-E/T_e),$$

where E is the electron energy. Then, the ionization rate can be written as

$$R_i(T_e)=\frac{8\pi}{m_e^2}\int_0^\infty \sigma_i(E)Ef_e(E)dE, \tag{A1}$$

where $\sigma_i(E)$ is the ionization cross-section. Figure 4(a) compares, for xenon, the experimental values of $\sigma_i(E)$ with the simple expression

$$\sigma_i(E)=\sigma_{i0}[1-\exp(E/E_i-1)], \tag{A2}$$

for $E>E_i$, with E_i the energy for primary ionization, and σ_{i0} a constant; $\sigma_i(E)=0$ for $E<E_i$. Equation (A2) turns to be a good approximation for electron energies E up to 100 eV, which is the range of interest for a Hall thruster. Substituting f_e and σ_i in Eq. (A1), one obtains

$$R_i(T_e)=\overline{\sigma_i}(T_e)\overline{c_e},$$

Downloaded 07 Jun 2001 to 138.4.73.144. Redistribution subject to AIP license or copyright, see http://ojps.aip.org/pop/popcr.jsp

$$\overline{\sigma_i}(T_e)=\sigma_{i0}\left(1+\frac{T_e E_i}{(T_e+E_i)^2}\right)\exp\left(-\frac{E_i}{T_e}\right), \tag{A3}$$

with $\overline{c_e}=\sqrt{8T_e/\pi m_e}$. Figure 4(b) compares this expression of $\overline{\sigma_i}(T_e)$ with the one obtained numerically from the experimental values. The agreement is very good up to $T_e \sim 40\,\mathrm{eV}$ and satisfactory up to $T_e \sim 100\,\mathrm{eV}$. Although it is easy to obtain better improvements with more complex expressions of $\sigma_i(E)$, we find it worthless for the objectives of the present model.

[1] A. Bishaev and V. Kim, Sov. Phys. Tech. Phys. **23**, 1055 (1978).
[2] G. Guerrini, C. Michaut, M. Dudeck, A. Vesselovzorov, and M. Bacal, in the *25th International Electric Propulsion Conference*, Cleveland, OH (Electric Rocket Propulsion Society, Cleveland, OH, 1997), IEPC Paper No. 97-053.
[3] J. Haas and A. Gallimore, in the *26th International Electric Propulsion Conference, Kytakyushu*, Japan (Electric Rocket Propulsion Society, Cleveland, OH, 1999), IEPC Paper No. 99-078.
[4] J. Fife and M. Martínez-Sánchez, in *24th International Electric Propulsion Conference*, Moscow, Russia (Electric Rocket Propulsion Society, Cleveland, OH, 1995), IEPC Paper No. 95-240.
[5] V. Kim, J. Propul. Power **14**, 736 (1998).
[6] J. Sankovic, J. Hamley, and T. Hang, in Ref. 4, IEPC Paper No. 93-094.
[7] F. Darnon, M. Lyszyk, and A. Bouchoule, in *33rd Joint Propulsion Conference*, Seattle, WA (American Institute of Aeronautics and Astronautics, Washington, DC, 1997), AIAA Paper No. 97-3051.
[8] C. Lentz and M. Martínez-Sánchez, in *29th Joint Propulsion Conference*, Monterey, CA (American Institute of Aeronautics and Astronautics, Washington, DC, 1993), AIAA Paper No. 93-2491.
[9] K. Komurasaki, K. Mikami, and Y. Arakawa, J. Propul. Power **11**, 1317 (1995).
[10] A. Fruchtman and N. Fisch, in *34th Joint Propulsion Conference*, Cleveland, OH (American Institute of Aeronautics and Astronautics, Washington, DC, 1998), AIAA Paper No. 98-3500.
[11] J. Boeuf and L. Garrigues, J. Appl. Phys. **84**, 3541 (1998).
[12] M. Keidar and I. Boyd, J. Appl. Phys. **86**, 4786 (1999).
[13] D. Oh, D. Hasting, C. Marrese, J. Haas, and A. Gallimore, J. Propul. Power **15**, 345 (1999).
[14] E. Ahedo and M. Martínez-Sánchez, in Ref. 10, AIAA Paper No. 98-8788.
[15] M. Martínez-Sánchez, E. Ahedo, and R. Noguchi, in Ref. 3, IEPC Paper No. 99-105.
[16] E. Ahedo, P. Martínez, and M. Martínez-Sánchez, in the *36th Joint Propulsion Conference*, Huntsville, AL (American Institute of Aeronautics and Astronautics, Washington, DC, 2000), AIAA Paper No. 2000-3655.
[17] A. Morozov, Y. Esipchuk, G. Tilinin, A. Trofimov, Y. Sharov, and G. Y. Shchepkin, Sov. Phys. Tech. Phys. **17**, 38 (1972).
[18] N. Meezan and M. Capelli, in Ref. 16, AIAA Paper No. 2000-3420.
[19] J. Pollard and E. Beiting, in *SP-465: 3rd Spacecraft Propulsion Conference* (ESA Publications Division, Noordwijk, 2000), p. 789.
[20] R. Myers and D. Manzella, in the *23rd International Electric Propulsion Conference*, Seattle, WA (Electric Rocket Propulsion Society, Cleveland, OH, 1993), IEPC Paper No. 93-096.
[21] F. Darnon, in Ref. 16, AIAA Paper No. 2000-3525.
[22] D. Rapp and P. Englander-Golden, J. Chem. Phys. **43**, 1464 (1965).
[23] D. Mathur and C. Badrinathan, Phys. Rev. A **35**, 1033 (1987).

Downloaded 07 Jun 2001 to 138.4.73.144. Redistribution subject to AIP license or copyright, see http://ojps.aip.org/pop/popcr.jsp